Modal structure of a supersonic under-expanded jet

C. Pérez Arroyo[a], G. Daviller[b], G. Puigt[c], C. Airiau[d]

a. Centre Européen de Recherche et de Formation Avancée en Calcul Scientifique, 42 Av. Gaspard Coriolis, 31057 Toulouse Cedex 01, France, cparroyo@cerfacs.fr
b. Institut de Mécanique des Fluides de Toulouse, UMR 5502 CNRS/INPT-UPS, Allée du professeur Camille Soula, 31400 Toulouse, France, guillaume.daviller@imft.fr
c. Centre Européen de Recherche et de Formation Avancée en Calcul Scientifique, 42 Av. Gaspard Coriolis, 31057 Toulouse Cedex 01, France, guillaume.puigt@cerfacs.fr
d. Institut de Mécanique des Fluides de Toulouse, UMR 5502 CNRS/INPT-UPS, Allée du professeur Camille Soula, 31400 Toulouse, France, christophe.airiau@imft.fr

Résumé :

Le bruit de choc est un bruit particulier qui intervient lorsque qu'un jet n'est pas parfaitement détendu. On observe alors des cellules de choc en aval de la tuyère, composées d'onde de compression et de détente. Les interactions entre la turbulence et ces cellules de choc sont responsable de la génération du bruit de choc. Ce bruit se caractérise par une directivité marqué vers l'amont de l'écoulement ainsi qu'une forte intensité. Dans cette étude, nous nous intéressons à l'analyse modale de la structure d'un jet supersonique sous-détendu caractérisé par un nombre de Reynolds $Re = U_j D_j/\nu_j = 10^6$, calculé par simulation aux grandes échelles (SGE) à l'aide du code elsA développée par l'ONERA avec l'intégration de schémas d'ordre élevé du CERFACS.

Abstract :

Shock-cell noise is a particular noise that appears in imperfectly expanded jets. Under these expansion conditions a serie of expansions and compressions appears following a shock-cell type structure. The interaction between the vortices developed at the lip of the nozzle and the shock-cells generates what is known as shock-cell noise. This noise has the particularity to be propagated upstream with a higher intensity. This paper will focus on the azimuthal modal analysis of the jet and the near-field of a non-screeching supersonic axisymmetrical under-expanded jet at Reynolds $Re = U_j D_j/\nu_j = 10^6$. Large eddy simulations (LES) are carried out using the elsA code developed by ONERA and extended by CERFACS with high-order compact schemes.

Mots clefs : Aéroacoustique, jet sous-détendu, bruit de choc, modes azimutaux, SGE.

1 Introduction

The noise perceived in the aft-cabin for an aircraft at cruise conditions is mainly due to the turbofan jet. The pressure mismatch between the ambient air and the secondary stream of a turbofan engine leads to the formation of diamond-shaped shock-cells. This serie of expansion and compresion waves interacts with the vortical structures developing in the mixing layer of the jet. This interaction process generates intense noise components on top of the turbulent mixing noise, which makes supersonic jets noisier than their subsonic counterparts [1]. The result is a broadband shock-cell associated noise (BBSAN), radiated mainly in the forward direction, which impinges on the aircraft fuselage and it is then transmitted to the cabin.

In this paper, the shock-cell noise generated by an axisymmetrical under-expanded single jet at Mach number $M = 1.15$ and Reynolds number $Re = U_j D_j/\nu_j = 10^6$ is investigated using Large-Eddy Simulations (LES). The paper addresses in a first term, the code characteristics, simulation setup and procedure, and validation against experimental data. The second part of the paper focuses on the azimuthal modal behavior of the perturbations reaching the nozzle exit plane, *i.e* with a directivity of 180° at the Strouhal numbers close to the experimental screech peak. The shape (amplitude and phase) of these perturbations is shown throughout the jet in the frequency domain.

2 Numerical Formulation

The full compressible Navier-Stokes equations in skew-symmetric formulation are solved using a Finite Volume multi-block structured solver (***elsA*** software by ONERA [2]). The spatial scheme is based on the well-known implicit compact finite difference scheme of 6th order of Lele [3], extended to Finite Volumes by Fosso *et al.* [4]. The above scheme is stabilized by the compact filter of Visbal & Gaitonde [5] that is also used as an implicit subgrid-scale model for the present LES. Time integration is performed by a six-step 3rd order Runge-Kutta DRP scheme of Bogey and Bailly [6].

3 Under-expanded Jet Conditions

Time-dependent simulations are presented of a contoured convergent nozzle with exit diameter $D = 38.0mm$ and a modeled nozzle lip thickness of $t = 0.125D$. The nozzle is operated under-expanded at the stagnation to ambient pressure ratio $p_s/p_\infty = 2.27$. The modeled exit and ambient conditions match those in the experimental set-up of André [7]. The ambient conditions of the air are temperature $T_\infty = 288.15K$ and pressure $p_\infty = 98.0kPa$. The exit stagnation temperature of the jet is assumed to be equal to the ambient conditions. The flow at the nozzle exit is mainly axial but some vertical components appear due to the inclined inner shape of the nozzle. In addition, a small co-flow of $0.5m/s$ is added in order to help the convergence of the results.

4 Simulation Setup, Procedure and Validation

4.1 Simulation Setup

The numerical computation is initialized by a RANS simulation using the Spalart-Allmaras turbulence model [8]. The RANS solution is wall resolved in the inner and outer sections of the nozzle with a

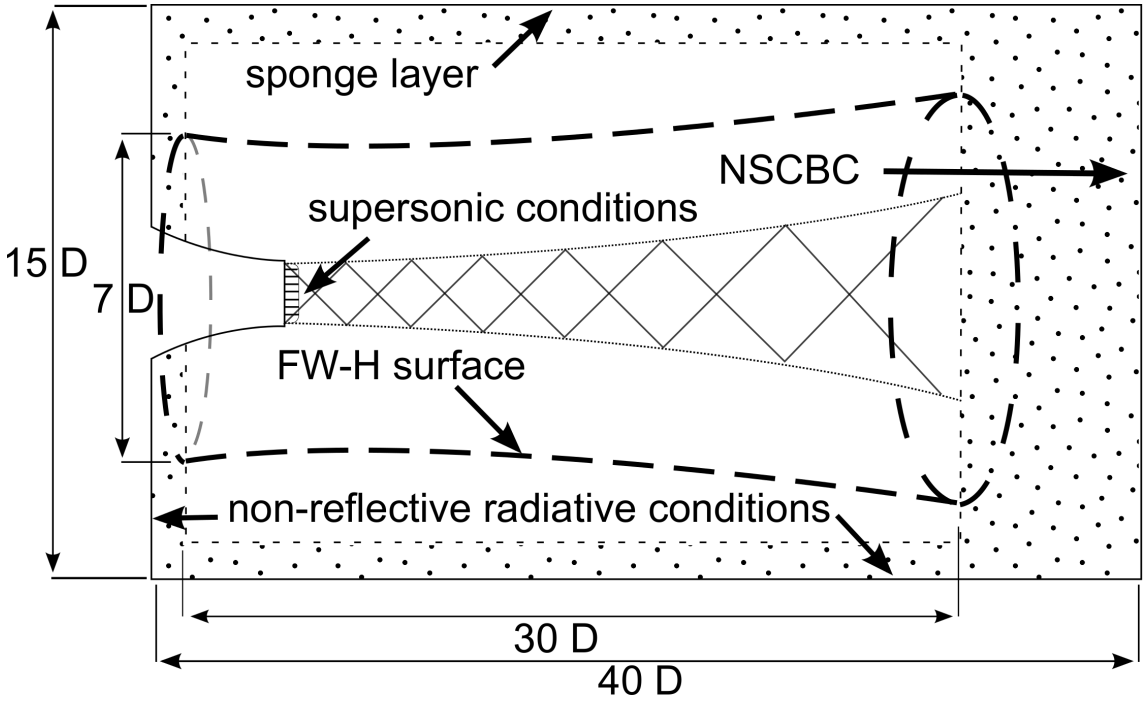

FIGURE 1 – *LES domain sketch*

$y^+ < 1$. Once the RANS simulation is mesh converged, the LES run is then initialized from the RANS simulation. The inner part of the nozzle is removed from the LES simulation and the RANS nozzle exit conservative variables are imposed [9, 10, 11, 12, 13, 14]. In addition, no inflow forcing is used. The mesh used in the LES simulation near the jet lip-line is coarsened in the radial direction with respect to the RANS mesh, meaning that no wall-resolution is achieved when the RANS solution is interpolated into the LES mesh. Nevertheless, the boundary layer at the exit of the nozzle is defined by 15 points. Each shock-cell is resolved within 40 cells in the axial direction.

The computational domain used for the LES simulation extends $40D$ in the axial direction and $7D$ in the radial direction as shown in Fig. 1. The mesh consists in 75×10^6 cells with $(1052 \times 270 \times 256)$ cells in the axial, radial and azimutal directions respectively. The maximum expansion ratio between adjacent cells achieved in the mesh is less than 4%.

Non-reflective boundary conditions of Tam and Dong [15] extended to three dimensions by Bogey and Bailly [16] are used in the exterior inlet as well as in the lateral boundaries. The exit condition is based on the characteristic formulation of Poinsot and Lele [17]. Furthermore, sponge layers are coupled around the domain to attenuate exiting vorticity waves. Due to the fact that the interior of the nozzle is not modeled, no inflow forcing is applied at the exit of the nozzle to avoid parasite noise.

4.2 Simulation Procedure

The simulation runs for 120 non-dimensional time units ($\hat{t} = tD/C_\infty$) in order to reach statistically independent results. After the transient phase, the simulation runs for $\hat{t} = 140$. The farfield sound is obtained by means of the Ffowcs-Williams & Hawkings analogy (FW-H) [18]. The surface used to extrapolate the variables to the farfield is located in a topological surface starting at $r/D = 3.5$ from the axis and growing with the mesh. The cut-off mesh Strouhal is $St = 2.0$ where $St = fD/U_j$. In terms of frequency, this value is defined as $f = c_\infty/(n\Delta)$, where Δ is the cell size, c_∞ the speed of sound

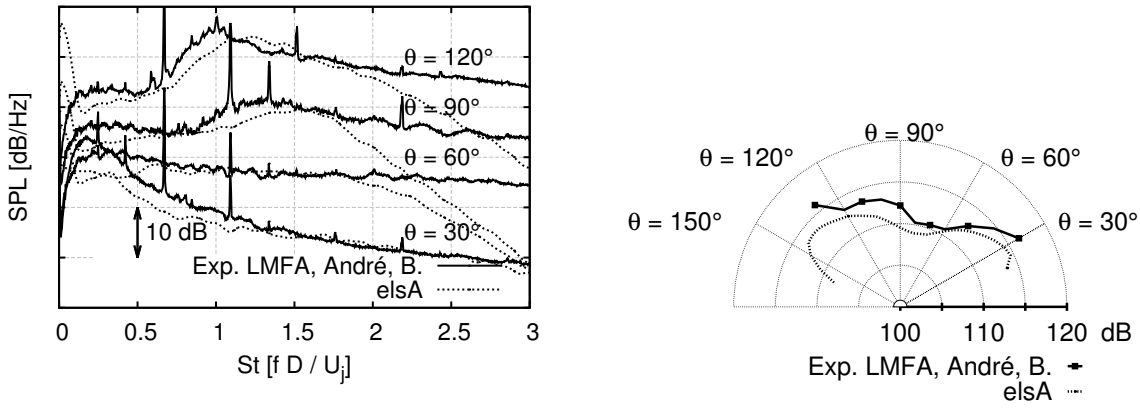

(a) (b)

FIGURE 2 – *Acoustic spectrum in the farfield (50 diameters) for a $M_j = 1.15$ under-expanded jet. θ is measured with respect to the jet axis, (a) SPL, (b) OASPL.*

and n the number of cells needed to resolve fluctuations with the numerical scheme used. The sampling frequency has been set to 100 kHz ($St = 5.0$).

4.3 Simulation Validation

The SPL at the farfield (50 diameters) propagated with the FW-H analogy is shown in Fig. 2 (a). An overall good agreement is obtained in amplitude for all the angles measured at the Strouhal range $0.5 \leq St \leq 2.0$ even when the turbulence length-scale is twice as the experimental one [19]. The disagreement found at low frequencies ($St \leq 0.5$) is mainly due to a lack of convergence of the statistics and the fact that the FW-H surface intersects the jet at the end of the domain, as explained by Bogey and Bailly [20]. The decay found at higher frequencies ($St \leq 2.0$) is the effect of the mesh constraints as explained in the previous section.

The overall sound pressure level (OASPL), computed at the Strouhal range $0.25 \leq St \leq 2.0$ for both experimental and numerical results is shown in Fig. 2 (b). The results differ from the experimental values at most 3dB. Both the lobe of the large structures at $30°$ and the lobe at $120°$ of the BBSAN are well captured.

5 Modal analysis

The discrete peaks found experimentally that can be seen in Fig. 2 are due to the phenomenon known as screech. This tonal noise appears due to a feedback loop between the pressure perturbations generated by the vortices impacting the shock-cells and the instabilities that generate these vortices at the lip of the nozzle. This phenomenon was not captured by the LES simulation due to the fact that the interior of the nozzle is not modeled [21, 22, 23]. Without it, the instabilities inside the shear-layer develop half a diameter downstream after a laminar region. Having the instabilities closer to the nozzle exit might help the presence of screech phenomenon as well, increasing the feedback loop gain because the lip acts as a reflecting boundary for the perturbations traveling upstream [24, 25].

Nevertheless, some phenomena related to the screech is captured. The total power spectral density (PSD) contained at the plane $z = 0$, *i.e* the sum of the PSD at every location $[x, y]$ for each frequency is shown in Fig. 3. A peak appears at $St = 0.62$, close to the experimental screech main tone ($St = 0.65$). The

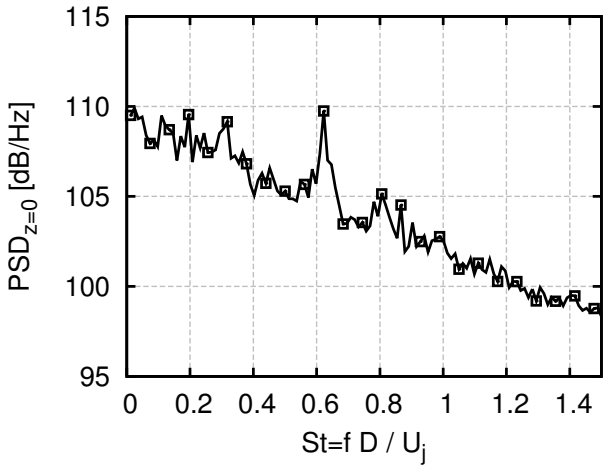

FIGURE 3 – *Total PSD contained at the plane z=0 for different frequencies*

Strouhal number obtained differs from the experimental one due to the lack of coupling between the perturbations propagating upstream and the vortices generated at the lip.

This Strouhal number and its vicinity will be the focus of the paper. In Fig. 4, the discrete Fourier transform (DFT) modulus of the plane $z/D = 0$ that was used to make the integral of Fig. 3 is shown at the $St = 0.62$. It is clear that some phenomena occurs near the axis, in the central region of the jet, mostly, due to the movement of the shock-cells, as a whole. The tips of the shock-cells, $i.e$ where the shock-cells impinge the shear layer, they also show a high power with respect to the rest of the jet, even if they do it with a lower intensity than the center. From the phase contours lines of Fig. 4, it can be established that there is a strong upstream directivity. A supersonic under-expanded screeching jet will show a similar amplitude in the screech (and some of its harmonics) for a wide range of angular positions (as it can be seen in the experimental results shown in Fig. 2). However, in order for the screech to occur, the feedback loop must be initiated with a strong noise radiation at $180°$ that will impact the region where the instabilities develop. In the following, the positions at $x/D = 0$ are studied in order to confine this phenomena only to acoustic perturbations without entering in the BBSAN main lobe region shown in Fig. 2 (b).

The PSD of the pressure is shown in Fig. 5 for different Strouhal numbers and different radius at the exit plane. The position closer to the jet ($r/D = 1$), Fig. 5 (a), shows clearly the tonal noise that occurs at $St = 0.62$ and a secondary peak at $St = 0.65$. The intensity of these two peaks is attenuated for the position $r/D = 2$ (Fig. 5 (b)) and non-relevant at $r/D = 3$ (Fig. 5 (c)) which is in agreement with a high upstream directivity ($\theta \approx 180°$) of the perturbations.

The azimuthal modal decomposition of the pressure at the same positions is shown in Fig. 6. The perturbations reaching the nozzle exit are composed of different modes for a wide range of Strouhal numbers. Close to the axis (Fig. 6 (a,d,g)), these modes alternate with the frequency. As explained for Fig. 5, although the modes are still distinguishable, an attenuation occurs at $x/D = 2$ (Fig. 6 (b,e,h)). However, farther away from the axis at $x/D = 3$ (Fig. 6 (c,f,i)), a position where the BBSAN starts to be important, the perturbations are composed of several superimposed modes for the frequency range of the shock-cell noise.

For the sake of clarity, the single values of the PSD are shown in Fig. 7 for the previous positions at the

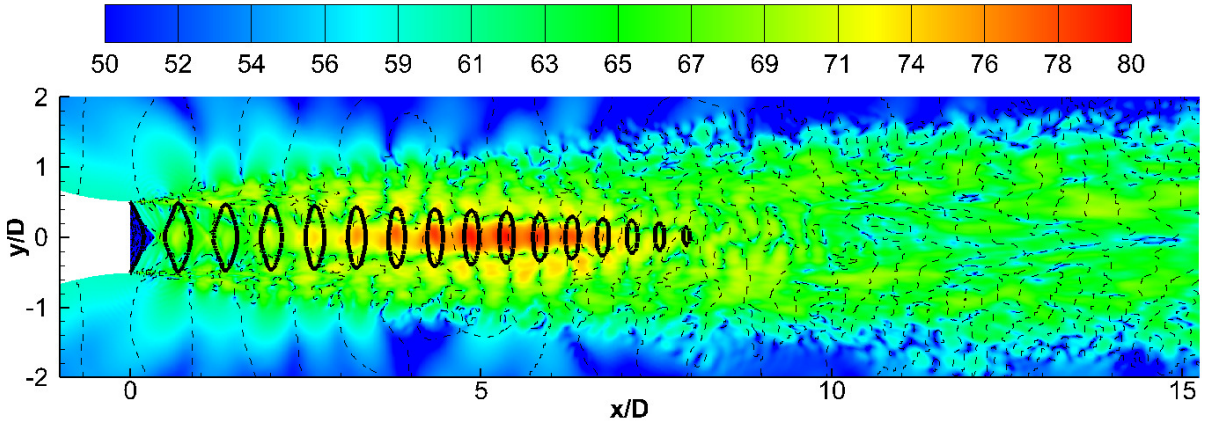

FIGURE 4 – *DFT modulus contours of pressure perturbations at* $z = 0$ *and* $St = 0.62$ *where the dashed lines are the contours of the phase at* $0°$ *and the solid lines represent the shock-cells.*

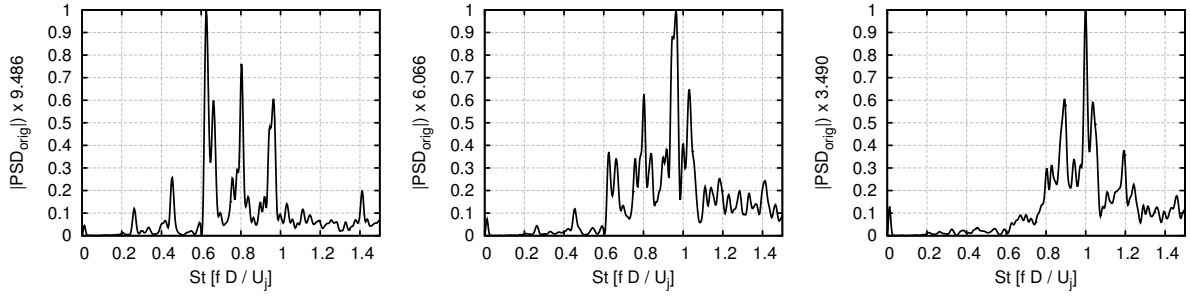

(a) (b) (c)

FIGURE 5 – *PSD of the pressure at the positions* $[x/D, r/D]$ *(a)* $[0, 1]$*, (b)* $[0, 2]$*, (c)* $[0, 3]$*. The ordinate axis is scaled by the maximum value.*

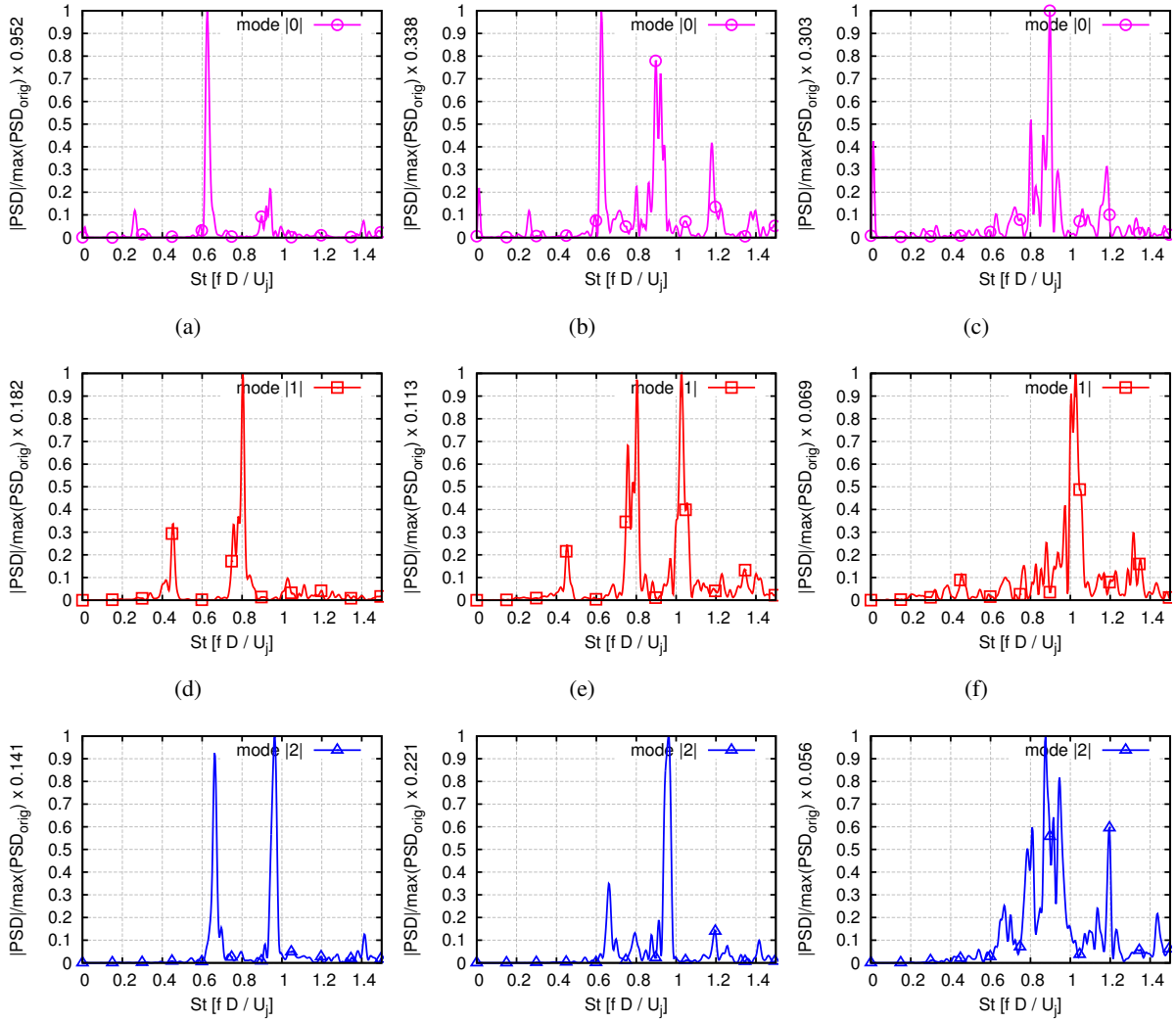

FIGURE 6 – *PSD of pressure of the azimuthal modes at the positions* $[x/D, y/D]$ *(a,d,g)* $[0, 1]$*, (b,e,h)* $[0, 2]$*, (c,f,i)* $[0, 3]$*, where the PSD has been averaged between positive and negative modes. The ordinate axis is scaled by the maximum value.*

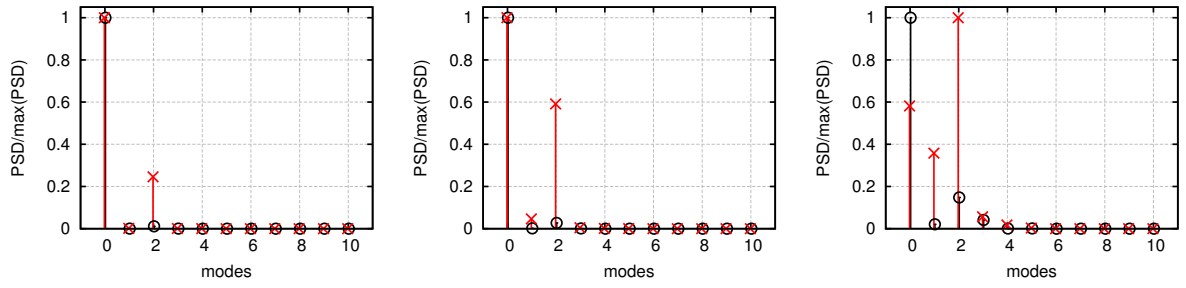

(a) (b) (c)

FIGURE 7 – *PSD of pressure of the azimuthal modes at* $St = 0.62$ *and* $St = 0.65$ *in* $\circ$ *and* $\times$ *respectivelyat the positions* $[x/D, y/D]$ *(a,d,g)* $[0, 1]$*, (b,e,h)* $[0, 2]$*, (c,f,i)* $[0, 3]$*, where the PSD has been averaged between positive and negative modes.*

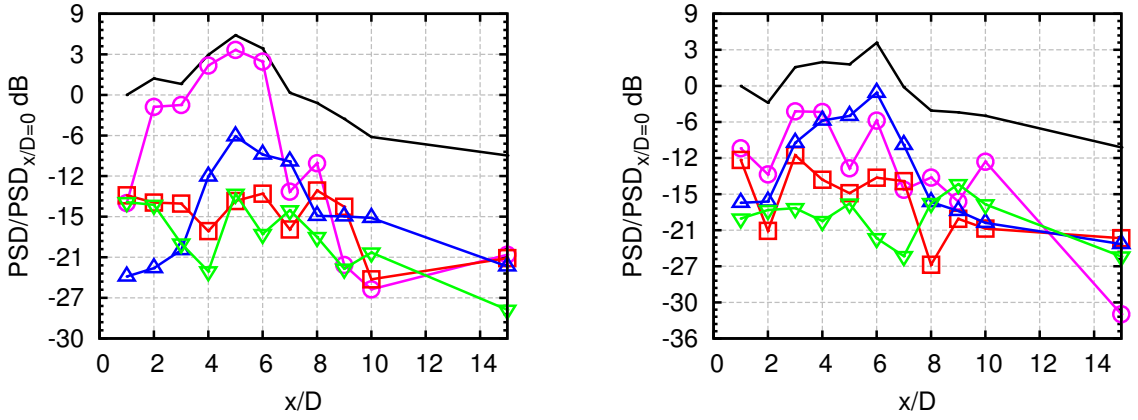

(a) (b)

FIGURE 8 – *PSD of pressure of the azimuthal modes at (a)* $St = 0.62$ *and (b)* $St = 0.65$ *at* $y/D = 0.5$*. The complete signal is shown in solid black line. The modes 0, 1, 2 and 3 are shown as* $\circ$*,* $\square$*,*$\triangle$ *and* $\triangledown$ *respectively, where the PSD has been averaged between positive and negative modes.*

Strouhal numbers of interest 0.62 and 0.65. The dominant mode at $St = 0.62$ is fully axisymmetrical (mode 0) whereas, at $St = 0.65$, a composition of axisymmetrical and helical modes appears. At the first two positions (Fig. 7 (a,b)), the axisymmetrical mode is dominant. However, at the farthest position (Fig. 7 (c)), the dominant mode changes to the second helical mode.

The previous figures 5, 6 and 7 all show that the modes are distinct close to the jet axis, outside the main lobe of the BBSAN shown in Fig. 2 (b) that is directed upstream, and with the same orders of magnitude otherwise. The PSD of the modes at the lip-line is shown in Fig. 8 for both Strouhal numbers. At $St = 0.62$, the contribution of the axisymmetrical mode 0, reaches the maximum at $x/D = 5$ and is dominant up to $x/D = 6$, farther downstream all the modes appear mixed with same order of magnitude. At $St = 0.65$, the dominance of the axisymmetrical mode 0 is lost downstream of $x/D = 4$ in favor of the helical mode 2, reaching the maximum at $x/D = 6$, again, farther downstream all the modes appear superimposed.

As it can be drawn from Fig. 3, in order to identify the peak around $St = 0.62$ the total energy contained must be higher than its surroundings, frequency wise. The modal decomposition at the lip-line can be applied to the root mean square (rms) in order to identify where are these modes contributing to the total spectra, or on this case, to the rms of the complete signal. Figure 9 (a) shows how the peak of the mode

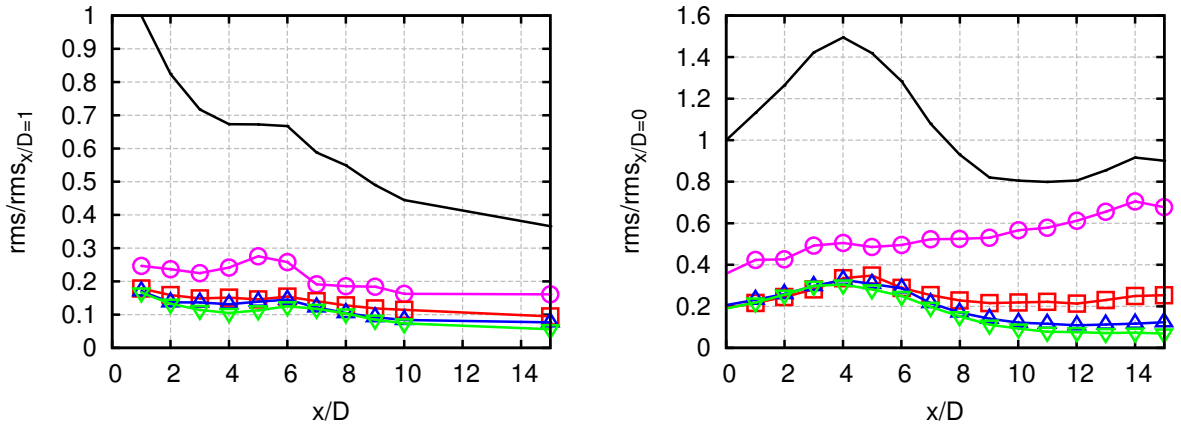

(a) (b)

FIGURE 9 – *RMS of pressure of the azimuthal modes at (a) $y/D = 0.5$ and (b) $y/D = 3$ (b). The complete signal is shown in solid black line. The modes 0, 1, 2 and 3 are shown as ○, □, △ and ▽ respectively, where the PSD has been averaged between positive and negative modes.*

0 lays on $x/D = 5$ and the peak of the axisymmetrical modes lay on $x/D = 6$ in agreement with Fig. 8. Figure 9 (b) shows that the behavior changes due to the BBSAN components that reach this region ($y/D = 3$). The peak at $x/D = 4$ of the mode 0 is almost flat, while the peaks of the rest of the modes are clearly visible.

Finally, in order to visualize the axisymmetrical and helical modes, the DFT modulus is shown for several axial positions in Fig. 10 and 11 at Strouhal 0.62 and 0.65 respectively. Suda et al. [26] reported high oscillations of the shock-cells for a rectangular supersonic screeching jet. Figures 10 and 11 show this mixed motion between axisymmetrical and helical modes for a circular supersonic non-screeching jet. At $St = 0.62$ the central part of the jet and the tips of the shock-cells oscillate in time axisymmetrically with the same phase and an annular region near the position of $M = 1.0$ that remains still. The helical behavior at $St = 0.65$ is presented with a cloverleaf pattern that alterns from negative to positive phases on each lobe.

6 Conclusions

A large eddy simulation of a supersonic under-expanded axisymmetrical jet has been carried out showing in Fig. 2 good agreement with the BBSAN and the OASPL against experimental results. Two azimuthal modes have been isolated for the frequencies in the vicinity of the experimental screech tone frequency showing an axisymmetrical and a helical behavior. These modes are radiated at a higher intensity at the angles close to the axis ($180°$) in agreement with the radiation pattern needed for the screech to appear. These modes are visible when plotting the DFT modulus and phase at different axial positions as seen in Fig. 10 and 11.

The perturbations reaching the nozzle exit are in agreement with the generation of screech tones. However, screech is not captured due to a lack of coupling between these perturbations and the instabilities of the shear layer. In order to close the feedback loop, the interior of the nozzle should be modeled. Nonetheless, this procedure allows to study the BBSAN without taking into account the impact that the screech tones have on the flow [27].

A large eddy simulation of a dual jet will be carried out following the same strategy in order to mimic, in a simplipied fashion, the jets of commercial aircrafts where the BBSAN appears isolated.

Acknowledgments

The authors are grateful for the experimental data provided by B. André and C. Bailly, from the Laboratoire de Mécanique des Fluides et d'Acoustique from Lyon, France.

This research project has been supported by a Marie Curie Initial Training Networks (ITN) AeroTraNet 2 of the European Community's Seventh Framework Programme (FP7) under contract number PITN-GA-2012-317142 that aims to generate a ready to use model for shock-cell noise characterization.

This work was performed using HPC resources from GENCI - [CCRT/CINES/IDRIS] (Grant 2015-[x20152a6074]).

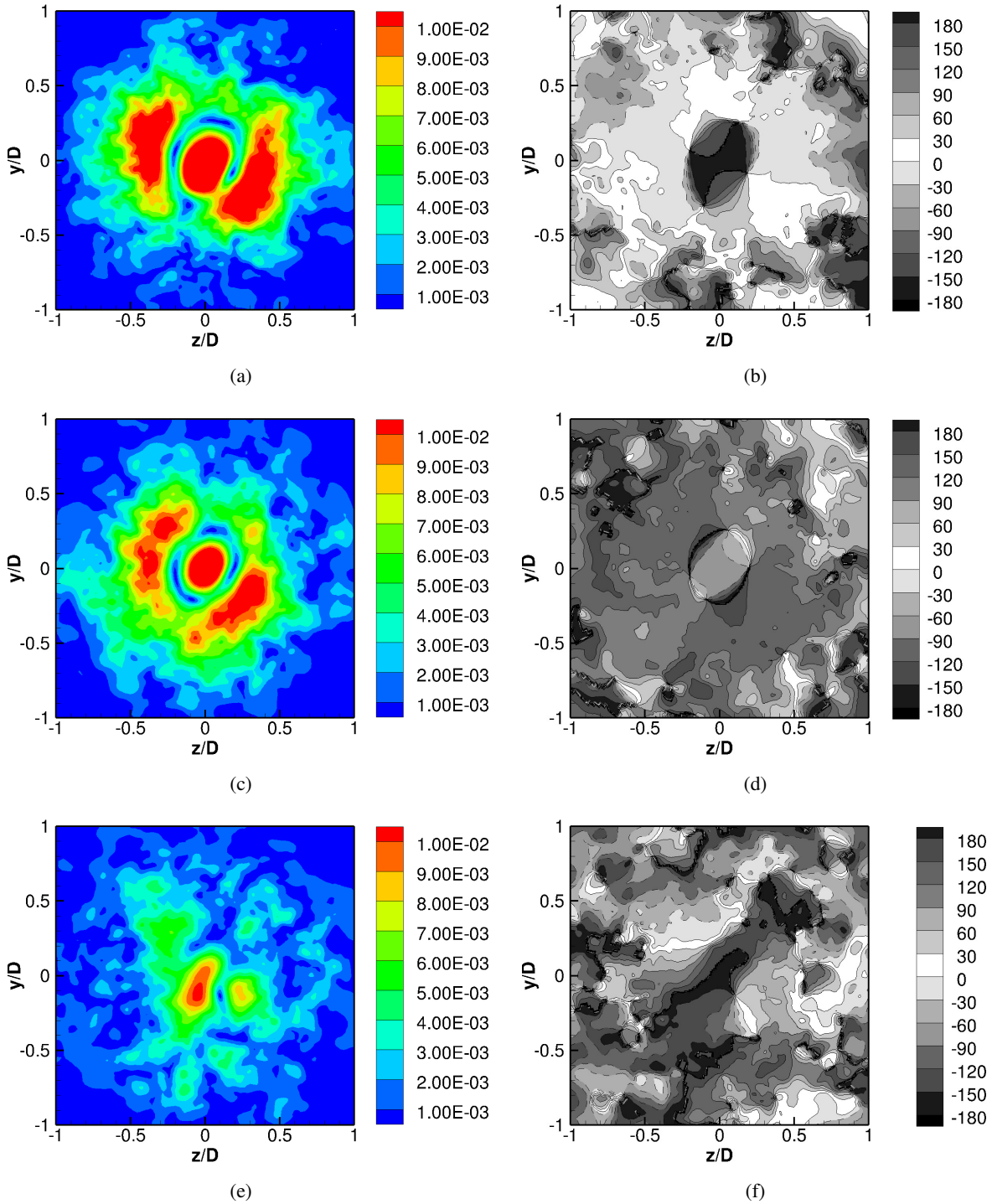

FIGURE 10 – *DFT modulus of the non-dimensional pressure ($\hat{p} = p/p_{ref}/\gamma$) and its phase on the left and right columns respectively at $St = 0.62$ at the planes (a,b) $x/D = 5$, (b,c) $x/D = 6$, (c,d) $x/D = 7$. The negative values of the phase are represented with dashed isolines.*

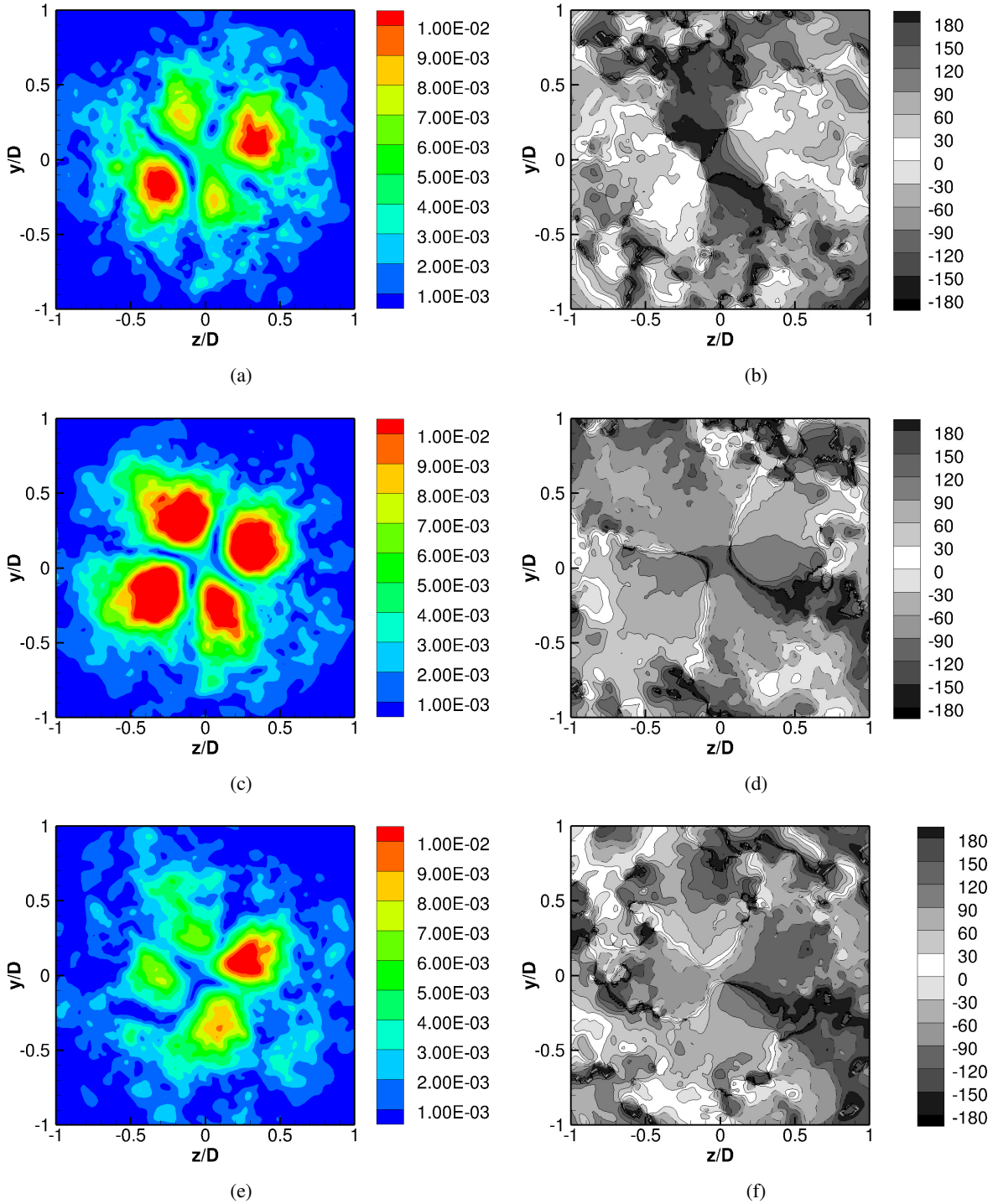

FIGURE 11 – *DFT modulus of the non-dimensional pressure ($\hat{p} = p/p_{ref}/\gamma$) and its phase on the left and right columns respectively at $St = 0.65$ at the planes (a,b) $x/D = 5$, (b,c) $x/D = 6$, (c,d) $x/D = 7$. The negative values of the phase are represented with dashed isolines.*

Références

[1] C. K. Tam, "Supersonic jet noise," *Annu. Rev. of Fluid Mech.*, vol. 27, no. 1, pp. 17–43, 1995.

[2] L. Cambier, S. Heib, and S. Plot, "The Onera elsA CFD software : input from research and feedback from industry," *Mech. & Ind.*, vol. 14, no. 03, pp. 159–174, 2013.

[3] S. Lele, "Compact finite difference schemes with spectral-like resolution," *J. Comput. Phys.*, vol. 103, pp. 16–42, 1992.

[4] A. Fosso-Pouangué, H. Deniau, F. Sicot, and P. Sagaut, "Curvilinear finite volume schemes using high order compact interpolation," *J. Comput. Phys.*, vol. 229, no. 13, pp. 5090–5122, 2010. jx.

[5] M. Visbal and D. Gaitonde, "On the use of higher-order finite-difference schemes on curvilinear and deforming meshes," *J. Comput. Phys.*, vol. 181, pp. 155–185, 2002.

[6] C. Bogey and C. Bailly, "A family of low dispersive and low dissipative explicit schemes for flow and noise computations," *J. Comput. Phys.*, vol. 194, no. 1, pp. 194–214, 2004.

[7] B. André, *Etude expérimentale de l'effet du vol sur le bruit de choc de jets supersoniques sous-détendus*. PhD thesis, L'École Centrale de Lyon, 2012.

[8] P. Spalart and S. Allmaras, "A one-equation turbulence model for aerodynamic flows," *AIAA Paper 92-0439, 30th Aerospace Sciences Meeting and Exhibit, Reno, Nevada (1992)*, 1992.

[9] T. Suzuki and S. K. Lele, "Shock leakage through an unsteady vortex-laden mixing layer : application to jet screech," *J. Fluid Mech.*, vol. 490, pp. 139–167, 2003.

[10] K. Viswanathan, M. Shur, M. Strelets, and P. R. Spalart, "Numerical prediction of noise from round and beveled nozzles," in *Turbulent Flow and Noise Generation, EUROMECH Colloquium 467, Marseille, France*, 2005. Turbulent Flow and Noise Generation, EUROMECH Colloquium 467, Marseille, France.

[11] M. Shur, P. Spalart, and M. Strelets, "Noise prediction for increasingly complex jets. part i : Methods and tests," *Int. J. Aeroacoustics*, vol. 4, no. 3 & 4, pp. 213–246, 2005.

[12] M. L. Shur, P. R. Spalart, M. K. Strelets, and A. V. Garbaruk, "Further steps in les-based noise prediction for complex jets," in *44th AIAA Aerospace Sciences Meeting and Exhibit, 9 - 12 January 2006, Reno, Nevada, AIAA Paper 2006-485*, vol. 485, p. 2006, 2006.

[13] C. Schaupp, J. Sesterhenn, and R. Friedrich, "On a method for direct numerical simulation of shear layer/compression wave interaction for aeroacoustic investigations," *Comput. Fluids*, vol. 37, no. 4, pp. 463–474, 2008.

[14] J. Schulze, J. Sesterhenn, P. Schmid, C. Bogey, N. de Cacqueray, J. Berland, and C. Bailly, "Numerical simulation of supersonic jet noise," pp. 29–46, Springer, 2009. Numerical Simulation of Turbulent Flows and Noise Generation.

[15] C. Tam and Z. Dong, "Radiation and outflow boundary conditions for direct computation of acoustic and flow disturbances in a nonuniform mean flow," *J. Comput. Phys.*, vol. 4, no. 02, pp. 175–201, 1996.

[16] C. Bogey and C. Bailly, "Three-dimensional non-reflective boundary conditions for acoustic simulations : far field formulation and validation test cases," *Acta Acust.*, vol. 88, no. 4, pp. 463–471, 2002.

[17] T. Poinsot and S. Lele, "Boundary conditions for direct simulations of compressible viscous flows," *J. Comput. Phys.*, vol. 101, pp. 104–129, 1992.

[18] F. Farassat and G. P. Succi, "The prediction of helicopter rotor discrete frequency noise," in *American Helicopter Society, Annual Forum, 38th, Anaheim, CA, May 4-7, 1982, Proceedings.(A82-40505 20-01) Washington, DC, American Helicopter Society, 1982, p. 497-507.*, vol. 1, pp. 497–507, 1982.

[19] C. Pérez Arroyo, G. Daviller, G. Puigt, and C. Airiau, "Shock-cell noise of supersonic under expanded jets," in *50th 3AF International Conference on Applied Aerodynamics*, (Toulouse, France), 29-30 March - 1 April 2015. conf.

[20] C. Bogey and C. Bailly, "Influence of nozzle-exit boundary-layer conditions on the flow and acoustic fields of initially laminar jets," *J. Fluid Mech.*, vol. 663, pp. 507–538, 2010.

[21] J. Berland, C. Bogey, and C. Bailly, "Large eddy simulation of screech tone generation in a planar underexpanded jet," in *12th AIAA/CEAS Aeroacoustics Conference (27th AIAA Aeroacoustics Conference 8–10 May 2006, Cambridge, Massachusetts*, pp. 8–10, 2006.

[22] A. Singh and A. Chatterjee, "Numerical prediction of supersonic jet screech frequency," *Shock Waves*, vol. 17, no. 4, pp. 263–272, 2007.

[23] J. Schulze and J. Sesterhenn, "Numerical simulation of supersonic jet-noise," *Proceed. Ap. Math Mech.*, vol. 8, no. 1, pp. 10703–10704, 2008.

[24] A. Powell, Y. Umeda, and R. Ishii, "Observations of the oscillation modes of choked circular jets," *J. Acoust. Soc. Am.*, vol. 92, no. 5, pp. 2823–2836, 1992.

[25] T. Norum, "Screech suppression in supersonic jets," *AIAA J.*, vol. 21, no. 2, pp. 235–240, 1983.

[26] H. Suda, T. A. Manning, and S. Kaji, "Transition of oscillation modes of rectangular supersonic jet in screech," in *AIAA, Aeroacoustics Conference, 15 th, Long Beach, CA*, 1993.

[27] B. André, T. Castelain, and C. Bailly, "Broadband shock-associated noise in screeching and non-screeching underexpanded supersonic jets," *AIAA J.*, vol. 51, no. 3, pp. 665–673, 2013.